Seismic attenuation from VSP data in methane hydrate-bearing sediments*

Jun Matsushima

7-3-1 Hongo Bunky-ku, Tokyo, 113-8656, Japan. Email: jun-matsushima@geosys.t.u-tokyo.ac.jp

Abstract. Recent seismic surveys have shown that the presence of methane hydrate (MH) in sediments has significant influence on seismic attenuation. I have used vertical seismic profile (VSP) data from a Nankai Trough exploratory well, offshore Tokai in central Japan, to estimate compressional attenuation in MH-bearing sediments at seismic frequencies of 30–110 Hz. The use of two different measurement methods (spectral ratio and centroid frequency shift methods) provides an opportunity to validate the attenuation measurements. The sensitivity of attenuation analyses to different depth intervals, borehole irregularities, and different frequency ranges was also examined to validate the stability of attenuation estimation. I found no significant compressional attenuation in MH-bearing sediments at seismic frequencies. Macroscopically, the peaks of highest attenuation in the seismic frequency range correspond to low-saturation gas zones. In contrast, high compressional attenuation zones in the sonic frequency range (10–20 kHz) are associated with the presence of methane hydrates at the same well locations. Thus, this study demonstrated the frequency-dependence of attenuation in MH-bearing sediments; MH-bearing sediments cause attenuation in the sonic frequency range rather than the seismic frequency range. As a possible reason why seismic frequencies in the 30–110 Hz range were not affected in MH-bearing sediments, I point out the effect of thin layering of MH-bearing zones.

Key words: methane hydrate, attenuation, VSP, free gas, Nankai Trough.

Introduction

Methane hydrates (MH), which form in marine sediments at water depths greater than a few hundred metres, are naturally occurring ice-like crystalline solids composed of methane molecules surrounded by water molecules (Sloan, 1990). Marine MH deposits are considered important in terms of their effect on global warming and sea floor stability, and as a potential energy resource. The formation of submarine MH is controlled by specific temperature and pressure conditions. MH-bearing marine sediments have long been seismically identified because of the presence of free gas below the methane hydrate stability zone, by prominent bottom simulating reflectors (BSRs) that mark the velocity contrast between MH-bearing sediment and sediment that contains free gas or water. BSRs are easily recognised in most marine seismic reflection profiles. Once we know that a MH zone exists, from the extent of the BSR, we are then interested in characterising the MH-bearing sediment and estimating the amount of MH within the sediment.

Several authors have estimated the amount of MH from seismic velocity data (e.g. Wood et al., 1994; Korenaga et al., 1997; Ecker et al., 2000), as MH within sediment pore space stiffens the sediment and results in an increase in seismic velocity. Although seismic velocity is potentially a useful indicator of MH concentration, seismic velocity is also strongly affected by the micro-scale MH distribution in pore spaces. Studies of rock physics indicate that if the hydrate forms at grain contacts it may act as a component of the load-bearing sediment framework and stiffen the sediment framework (e.g. Helgerud et al., 1999). In this case, both compressional and shear wave velocities will increase dramatically, even if MH occupies only a few percent of the pore space.

While the presence of MH increases the seismic velocity of the host sediment, recent work on sonic logging data shows that sonic waveforms are also significantly affected by the presence of MH (Guerin and Goldberg, 2002; Matsushima, 2004). The combined use of velocity and attenuation data provides greater insight into the MH-bearing sediments. Guerin and Goldberg (2002) used monopole and dipole waveforms to calculate intrinsic sonic attenuation, and derived the first empirical relationship between sonic attenuation and MH concentration of sub-permafrost MH-bearing sediments within the Mackenzie delta, Canada. At the same field, Pratt et al. (2003) used crosshole seismic data with a frequency content of 150–500 Hz to obtain an attenuation tomogram, using waveform tomography techniques. These authors also found a strong correlation between attenuation and velocity in the MH-bearing sediments. Matsushima (2004) used full waveform logs from the Nankai Trough exploratory well off central Japan to estimate both compressional and shear attenuation in MH-bearing sediments. These attenuation estimates were based on the median frequency shift method described by Guerin and Goldberg (2002). Matsushima (2004) analysed attenuation at sonic frequencies of 10–20 kHz for compressional waves and 500–1000 Hz for shear waves, and observed that the presence of MH increases the seismic attenuation in the host sediment. The increase of attenuation with increasing velocity is somewhat unintuitive. It is important to accumulate attenuation measurements on MH-bearing materials in various frequency bands and in various geologic environments in order to determine the physical model that best describes these phenomena.

Few measurements of attenuation in MH-bearing sediments have been undertaken at seismic frequencies over the range

---

of distances relevant to seismic prospecting. Vertical seismic profile (VSP) measurement is considered to be best suited for attenuation studies as it enables sampling of the downgoing wavefield at various known depths (Matsushima, 2006). The downgoing waveform in a zero-offset VSP dataset provides direct observations of the changing nature of the source wavelet as it propagates through the earth. Matsushima (2006) estimated compressional attenuation from two VSPs using both the spectral ratio and centroid frequency shift methods. To remove the effect of intrabed multiples from the total attenuation, the author computed the attenuation from multiples using synthetic seismic modelling and subtracted the scattering attenuation from total attenuation. The final attenuation results indicate that high attenuation over the seismic frequency range (30–110 Hz) is associated with the presence of probable gas zones, while significant compressional attenuation was not observed in MH-bearing sediments at seismic frequencies. In this paper, I use the same zero-offset VSP data obtained as used in Matsushima (2006), to calculate the intrinsic attenuation at seismic frequencies. The sensitivity of attenuation analyses to different depth intervals, borehole irregularities, and different frequency ranges is also examined to validate the stability of attenuation estimation.

Field description and VSP data

The Nankai Trough is the bathymetric expression of the convergent boundary between the subducting Philippine Sea plate and the Eurasian plate in central and south-west Japan (Figure 1). Along the trough, several forearc basins and accretionary prisms have developed, and bottom-simulating reflectors (BSRs) are widely recognised within these structures. Based on the identification of BSRs, a campaign to drill exploratory wells and confirm the presence of MH reservoirs was undertaken between late 1999 and early 2000 by the Japanese Ministry of International Trade and Industry (MITI; Figure 1). Six wells were drilled during the campaign, including the main well, two pilot wells, and three post-survey wells spaced at intervals of 10–100 m (Figure 1); details of the drilling program can be found in Tsuji et al. (2004). Figure 2 shows a depth-converted 2D seismic profile across one of the MITI wells. The seismic profile clearly reveals a strong BSR feature at 1200–1400 m depth. An unusual pattern consisting of two

separate reflectors (upper and lower) can be distinguished, which has been termed a double BSR (Inamori and Hato, 2004).

The drilling and logging programs for the MITI Nankai Trough wells were designed to acquire cores and a complete suite of log data including caliper, gamma ray, nuclear magnetic resonance (NMR), neutron porosity, density, resistivity, full waveform sonic, and VSP (zero-offset, offset, and walk-away) data. Wireline logging surveys, including VSP surveys, were conducted at three wells (Main Hole, Post Survey Well 1, and Post Survey Well 3). In this study we use the zero-offset VSP data obtained from Post Survey Well 1 (PSW1).

VSP surveys were carried out at both PSW1 and PSW3 over a depth range of 1005–1305 m, with a recording interval of 5 m. The source was a GI gun arrangement designed to obtain broadband data. The source signal was recorded in an uncased borehole by a clamped three-component geophone, and the recording sample rate was 1 ms. In the following analysis, I use only the vertical component data of PSW1 at depths of 1050–1300 m (Figure 3a).

The traces were aligned at the first arrivals and a spatial averaging operation was performed using seven traces (weighting factor = 0.6, 1, 1, 1, 1, 1, 0.6), and finally primary downgoing waveforms were windowed with a cosine-tapered window (length = 50 ms) centred at the first peak (Figure 3b). The local reflectors in the vicinity of receivers have most effect on VSP data (Stainsby and Worthington, 1985). These reflecting structures can cause significant modulation in the observed amplitude spectra, making accurate Q estimates difficult to obtain. Therefore, the spatial averaging operation is generally applied to the original VSP data to obtain stable data without the effect of local small-scale reflectors around the receivers.

Methodology

We calculated the centroid frequency (f_c; Figure 4) for windowed waveforms at each depth as:

$$f_c = \frac{\int_0^\infty f A(f)\,df}{\int_0^\infty A(f)\,df} \tag{1}$$

where $A(f)$ is the spectral amplitude at frequency f. Figure 4 shows centroid frequency calculated from equation (1) as a
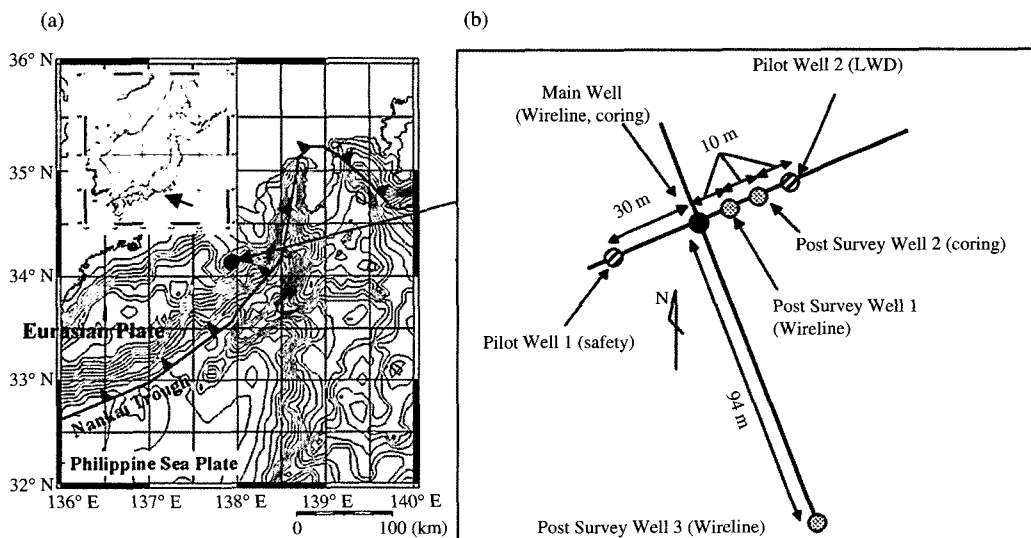
(a)   (b)

Fig. 1.   (a) Bathymetry and physiographic features of the eastern Nankai Trough and the location of MITI Nankai Trough wells. (b) Enlargement showing the configuration of the MITI Nankai Trough drilling campaign site.
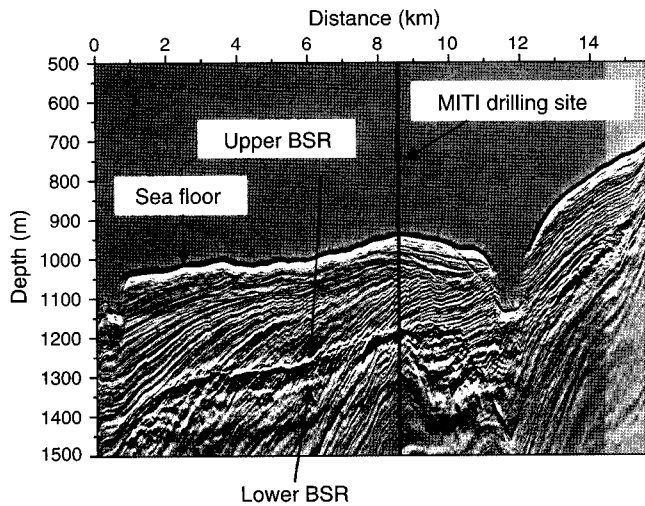
Fig. 2. Depth-converted seismic section across the MITI drilling campaign site. Double BSRs (upper and lower) can be recognised at around 1200–1400 m.
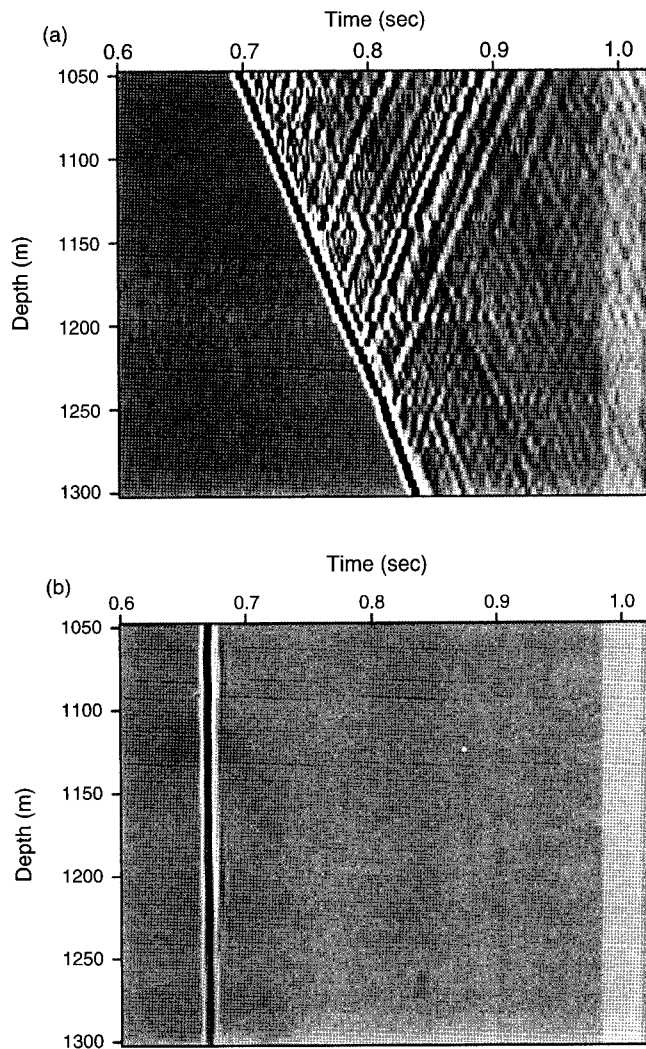
Fig. 3. (a) Variable-density displays of the vertical component of zero-offset VSP waveforms recorded at PSW1. Trace interval is 5 m. (b) After first arrival alignment, trace mixing using seven traces, and extraction by a cosine-tapered window (length = 50 ms).
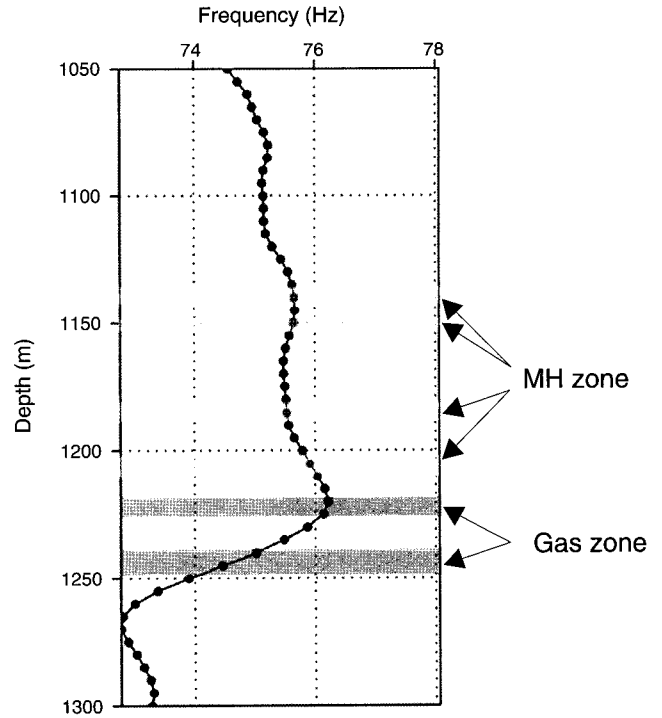
Fig. 4. Centroid frequency as a function of depth for each complete section of PSW1. Hydrate layers (light grey zones) and gas zones (dark grey zones) are overlaid on the figures.

function of depth. In Figure 4 hydrate layers (light grey zones) and gas zones (dark grey zones) are overlain on the figures. Two intervals are considered to contain a small amount of gas in the formation because the presence of gas affects the compressional wave. It can be seen that the centroid frequency significantly decreases below the gas-bearing zones.

The most popular method for estimating attenuation is based on spectral ratios, where data from two receiver depths straddling a medium of assumed constant Q are selected. The basis of the method is essentially that the logarithm of the spectral amplitude of a seismic wave decays at a rate roughly proportional to the frequency. Seismic wave attenuation can be modelled as the solution for a damped oscillating system as:

$$A(f, x_2) = B \cdot A(f, x_1)e^{-\pi f \Delta t/Q}, \tag{2}$$

where $A(f,x)$ is the amplitude spectrum at depth x, and Δt is the difference in arrival time between the two receiver depths. B is a constant that takes into account the source function, receiver function, and geometrical function. Rearranging equation (2) and taking the logarithm gives:

$$\ln\left|\frac{A(f, x_2)}{A(f, x_1)}\right| = -\pi f \Delta t/Q + C \tag{3}$$

A linear regression of the left hand side of equation (3) versus frequency therefore yields a slope that is equal to $-\pi \Delta t/Q$. C is a constant that takes into account the source function, receiver function, and geometrical spreading function. Equation (3) was applied to the windowed direct arrivals from the vertical component described above. The down-going arrivals at geophones at different depth intervals (20, 40, 60 m) were computed in a continuously sliding window to total depth. Here a depth interval is defined as the difference between x_1 and x_2 denoted in equation (3). Even though MH layers are thin, it is important to confirm how the attenuation estimates vary with depth interval.

Quan and Harris (1997) demonstrated that it is generally difficult to obtain reliable attenuation estimates from the amplitude decay method because amplitudes are easily contaminated by factors such as scattering effects, geometrical spreading, and source and receiver coupling. The authors proposed a method based on pulse broadening, using the estimated shift in the centroid of the pulse spectrum. The basis of the method is that the centroid frequency and variance of the first arrival wavelets are extracted and used to calculate attenuation. Quan and Harris (1997) derived a basic equation for attenuation estimation in the zero-offset VSP geometry. Q between the i-th and $(i+1)$-th receiver is defined by

$$Q_i = \frac{\pi \sigma_i^2 \Delta t_i}{\Delta f_i},\qquad(4)$$

where $\Delta f_i = (f_i - f_{i+1})$ is the centroid frequency difference between two depth levels, $\Delta t_i = (t_i - t_{i+1})$ is the travel time difference between the two levels, and σ_i^2 is the variance at the i-th receiver. Equation (4) was applied to the windowed direct arrivals on the vertical component described above. The down-going arrivals at geophones at different depth intervals (20, 40, 60 m) were computed in a continuously sliding window to total depth.

Attenuation estimation

Figure 5 shows total attenuation-depth profiles for the VSP data with different depth intervals from two different attenuation estimation methods. In Figure 5 three different profiles indicate the three different depth intervals. Attenuation analyses with different depth intervals seem to give consistent results. The highest attenuation zone corresponds to the principal gas zone. We can also see the physically unrealisable phenomenon of negative attenuation, which has been reported previously in VSP attenuation studies (e.g. Jannsen, Voss, and Theilen, 1985). Negative attenuation means that the amplitudes of high frequency components are increasing with depth. Possible reasons for this unphysical phenomenon might be a scattering effect, ambient noise, spectral distortion by windowing, and the choice of receiver separation. Figures 5a and 5b also show that
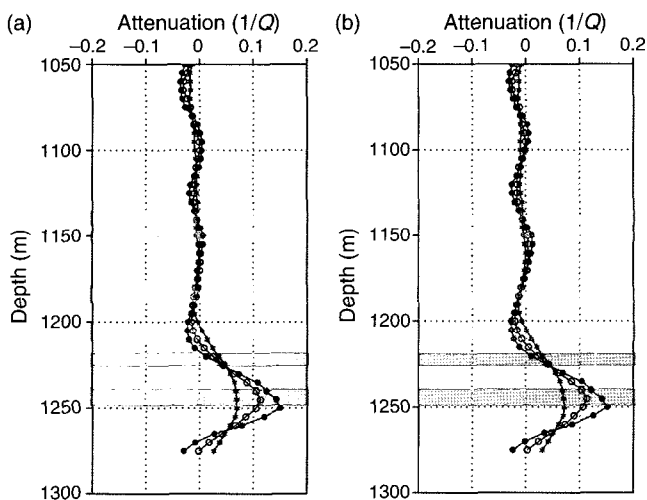
the spectral ratio and centroid frequency shift methods produce similar estimates of attenuation.

The attenuation results measured from VSP data are not entirely due to the intrinsic properties of the rock; a component of attenuation due to scattering effects is also included in the estimate. Here, attenuation from multiples is computed using synthetic seismic modelling and by subtracting the scattering attenuation from total attenuation. This removes the effect of intrabed multiples from the total attenuation. I assume that the scattering effect is due to intrabed multiples in 1D horizontal layering. Gist (1994) pointed out that a 1D model of layered stratigraphy significantly underestimates the scattering attenuation resulting from 3D heterogeneities; however, it is difficult to determine lateral heterogeneities such as variations in bed thickness.

A reflection response function for a 1D discretised earth model can be obtained using ray theory and Z-transforms via the Goupillaud model (Goupillaud, 1961). The input source wavelet is a unit spike and a bandpass filter (30–110 Hz) is applied to the output wavelet. The bandwidth of 30–110 Hz is consistent with the bandwidth for attenuation analysis. Receiver positions are the same as the actual VSP survey and the source position is located on the sea floor at 945 m. The reflection coefficient series is calculated using sonic and density logs from the well (Figure 6a). Figure 6b shows synthetic normal-incidence (zero-offset) VSP data.

The synthetic VSP data shown in Figure 6b were then analysed for attenuation using the same procedure applied to the field VSP data. Figures 7a and 7b show the estimates of scattering attenuation obtained by spectral ratio analysis and centroid frequency shift analysis, respectively. In Figure 7 three different profiles indicate three different depth intervals. Attenuation analyses with different depth intervals seem to give consistent results. Zones of higher attenuation correlate with the vicinity including the principal MH layers where intrabed multiple losses are much larger due to higher contrast of acoustic impedance. Tsuji et al. (2004) reported that the relatively thin MH-bearing zones, which typically lie within turbiditic sandy layers, are less than 1 m in thickness. The effect of this fine layering is to enhance the low frequency content of the downgoing wavelet relative to the higher frequencies (Pujol and Smithson, 1991). The high attenuation is caused by small-scale variations in acoustic impedance. There is little difference in the attenuation estimates of the spectral ratio and centroid frequency shift methods, and it is apparent that intrabed
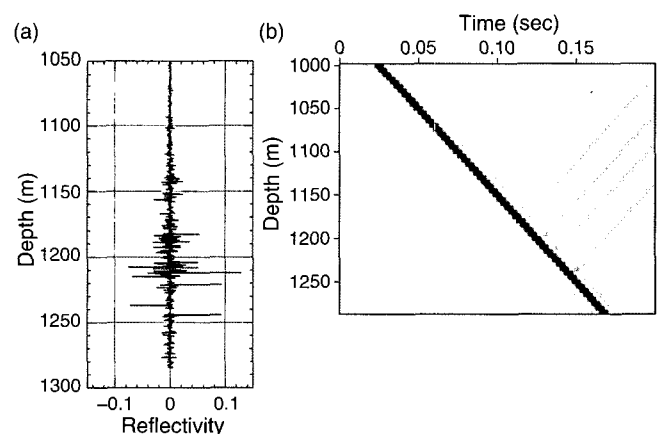

Fig. 5. Total attenuation-depth profiles for the VSP data with different depth intervals from two different attenuation estimation methods – spectral ratio and centroid frequency shift methods. Hydrate layers (light grey zones) and gas zones (dark grey zones) are overlain on the figures. (a) Using the spectral ratio method. (b) Using the centroid frequency shift method. Solid circles = depth interval of 20 m, open circle = 40 m, asterisk = 60 m.

Fig. 6. (a) Reflection coefficient series derived from velocity and density logs. (b) Synthetic zero-offset VSP data derived from the reflection coefficient series, using the Goupillaud model.

multiple losses in synthetic VSP data are much smaller than the observed attenuation.

Finally, the intrinsic attenuation was enhanced by subtracting the effect of intrabed multiples from the total attenuation. Figures 8a and 8b show the intrinsic attenuation estimates obtained via spectral ratio analysis and centroid frequency shift analysis, respectively. In Figure 8 three different profiles indicate three different depth intervals. Even after subtracting the scattering attenuation from total attenuation, the physically unrealisable phenomenon of negative attenuation could not be removed. The main reason for this could be the three-dimensional scattering effect, which still remains in the results that have been adjusted for intrinsic attenuation. I should estimate the scattering attenuation resulting from 3D heterogeneities; however, it is difficult to determine lateral heterogeneities such as variations in bed thickness. Other possible reasons for negative attenuation are ambient noise,

spectral distortion by windowing, source conditions, geophone coupling, and the choice of receiver separation.

To estimate the influence of borehole irregularities on the attenuation estimates, correlation coefficients are calculated in cross plots of caliper data and the VSP attenuation data: the correlation coefficient is $R^2 = 0.0001$ (Figure 9). This result shows that borehole irregularities have a minimal effect on the attenuation estimates. The sensitivity of attenuation analysis to different frequency ranges (30–110 Hz, 50–110 Hz, and 70–110 Hz) was also examined. Figures 10a and 10b show the intrinsic attenuation estimates which were obtained via spectral ratio analysis and centroid frequency shift analysis, respectively, for three different frequency ranges. In Figure 10 the three different profiles indicate three different depth intervals. This result shows that the choice of frequency range does not have a significant effect on the attenuation estimates for the seismic frequency ranges described above.
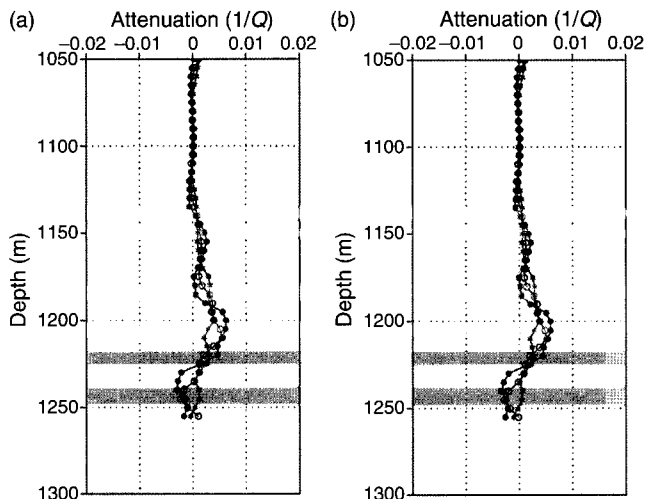
Discussion

I have calculated the intrinsic attenuation of the compressional wave in the seismic frequency range (30–110 Hz) from zero-

Fig. 7. Scattering attenuation-depth profiles for synthetic VSP data with different depth intervals from two different attenuation estimation methods – (a) spectral ratio and (b) centroid frequency shift methods. Hydrate layers (light grey zones) and gas zones (dark grey zones) are overlain on the figures. Solid circles = depth interval of 20 m, open circle = 40 m, asterisk = 60 m.
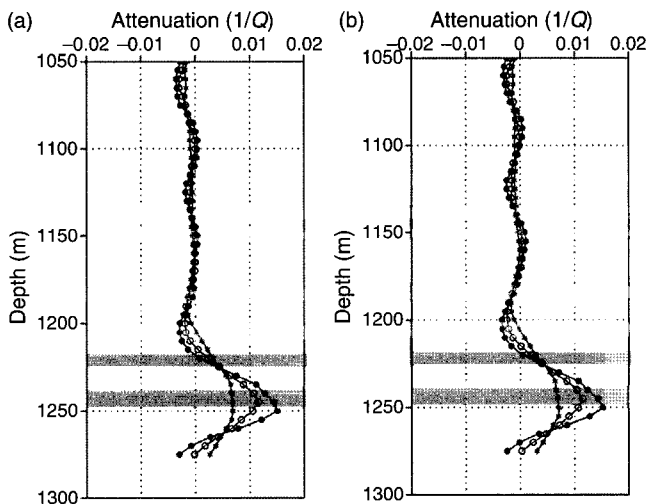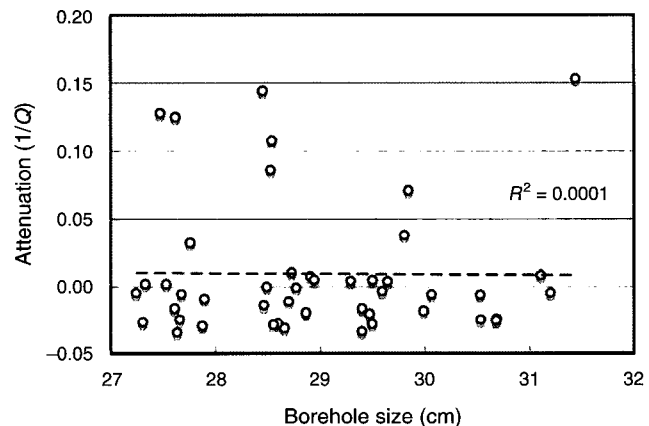

Fig. 9. Cross plots of seismic attenuation estimated from the VSP data and borehole size from the caliper log.

Fig. 8. Intrinsic attenuation-depth profiles for the VSP data with different depth intervals from two different attenuation estimation methods – (a) spectral ratio and (b) centroid frequency shift methods. Hydrate layers (light grey zones) and gas zones (dark grey zones) are overlain on the figures. Solid circles = depth interval of 20 m, open circle = 40 m, asterisk = 60 m.
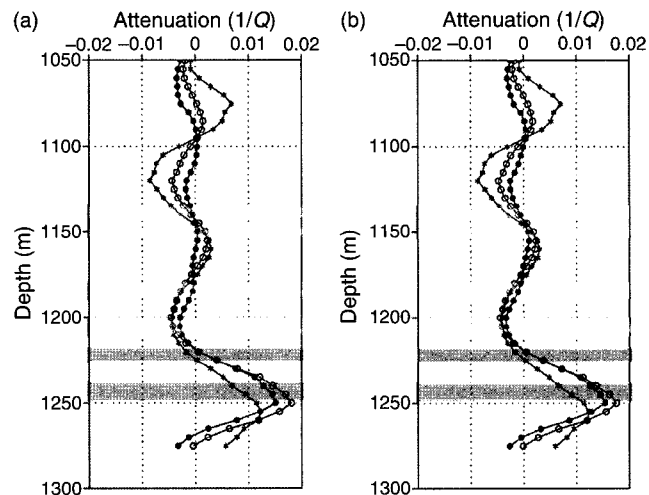

Fig. 10. Intrinsic attenuation-depth profiles for the VSP data with different frequency ranges from two different attenuation estimation methods – (a) spectral ratio and (b) centroid frequency shift methods. Hydrate layers (light grey zones) and gas zones (dark grey zones) are overlain on the figures. Solid circle = frequency range of 30–110 Hz, open circle = 50–110 Hz, asterisk = 70–110 Hz.

offset VSP waveforms. The sensitivity of attenuation analyses to different depth intervals, borehole irregularities, and different frequency ranges has also been examined to validate the stability of attenuation estimation. Macroscopically, the peaks of high attenuation in the seismic frequency range correspond to possible low-saturation gas zones. No significant compressional attenuation was observed in MH-bearing sediments at seismic frequencies. In contrast, zones of high compressional attenuation in the sonic frequency range (10–20 kHz) correspond to the presence of both MH and gas-saturated sediments (Matsushima, 2004). Combining the results from the present paper and the paper by Matsushima (2006), it is evident that the attenuation response in MH-bearing sediments is remarkably dependent on frequency. Strong attenuation is observed in the sonic frequency range, quite little in the seismic range.

In terms of a plausible mechanism for attenuation in MH-bearing sediments, we must consider the physical interactions between grains, pore fluid, and MH. Although there are several rock physics models to explain the effect of an increase of velocity with MH concentration (Lee et al., 1996; Helgerud et al., 1999; Gei and Carcione, 2003), there are only a few models to explain a mechanism for attenuation in MH-bearing sediments. Existing rock-physics models for attenuation are based on Biot's model (Biot, 1956) and its extension, because the physical interaction between grains, pore fluid, and MH is considered to be important for attenuation. Several authors assume that one of the main intrinsic seismic attenuation mechanisms is associated with wave-induced flow of the pore fluid. This flow is generated in a heterogeneous porous medium when a propagating seismic wave induces a local pore pressure gradient. Another possible attenuation mechanism is scattering (e.g. Kamei et al., 2004). While there are other possible mechanisms for attenuation in composite materials, including the effects of wetting on grain boundaries (Johnston et al., 1979), viscous shear relaxation (Walsh, 1969), and friction (Walsh, 1966), these mechanisms are generally unable to explain attenuation mechanisms in MH-bearing sediments (Chand and Minshull, 2004).

Dvorkin and Uden (2004) suggested that attenuation may result from macroscopic fluid cross-flow due to elastic wave excitation. The presence of thinly layered MH stiffens unconsolidated sediments, producing an elastic contrast between neighbouring MH-bearing and MH-free sediments. Higher elastic contrast between the layers results in stronger fluid cross-flow and greater attenuation of sonic waves. Dvorkin and Uden (2004) quantified the effect of macroscopic squirt flow on seismic wave attenuation based on a specific relationship between attenuation and frequency-related velocity change. This relation is known as the Kramers–Kronig equation, and states that greater attenuation is associated with a larger seismic velocity change between low and high frequency. The authors concluded that attenuation in MH-bearing sediments is due to self-induced elastic heterogeneity.

Chand and Minshull (2004) modelled attenuation in terms of Biot flow and squirt flow mechanisms in composite media, and found that contrast in permeability between the host sediment and MH produces attenuation in MH-bearing sediments. These authors used an approach based on self-consistent approximation and differential effective medium theory to relate the seismic properties of hydrate-bearing sediments to their porosity, mineralogy, microstructure, clay particle anisotropy, and hydrate saturation. Chand and Minshull (2004) estimated the attenuation effects due to the effects of fluid flow thorough sediments as well as the effects of fluid flow through MH; the MH is more permeable than sediment. Hydrate itself is porous and has its own fluid flow properties (e.g. Staykova et al., 2003). Variations in permeability alter both the magnitude of the attenuation and the frequency response. Attenuation increases due to a higher proportion of fluid flow in the hydrate matrix. The authors concluded that an increase in attenuation is primarily due to increased fluid flow within MH-bearing sediments. In an analysis of the Mallik 2L-38 well, Mackenzie Delta, Canada, Chand and Minshull (2004) concluded that the major influence on attenuation at frequencies above around 200 Hz is the effect of fluid flow within MH-bearing sediments.

According to the rock physical mechanism proposed by Chand and Minshull (2004), fluid flow within MH-sediments increases at the sonic log frequency range because pore-scale interactions between MHs, grains, and infilling fluid affect the sonic waveforms. The increment consequently results in high attenuation in MH-sediments. On the other hand, fluid flow in MH-sediments is much less at the seismic frequency (30–110 Hz) because such pore-scale interactions are negligible. It leads to low attenuation. These inferences obtained by their model well describe the observed facts shown in the present paper and in Matsushima (2004). Therefore, it is appropriate to explain my conclusions through the rock physical mechanism proposed by Chand and Minshull (2004).

Another possible reason why seismic scale frequencies are not affected in MH-bearing sediments might be the effect of thin layering of MH-bearing zones. Tsuji et al. (2004) described thin MH-bearing zones that typically lie within turbiditic sandy layers that are less than 1 m in thickness, and the total thickness of MH-bearing zones is ~14 m. Such thicknesses may be to small to affect waves at seismic frequencies. Further resolution analysis is needed to clarify the effect of thin layering of MH-bearing zones.

Conclusions

In this paper, I have estimated compressional attenuation from the VSP data using both the spectral ratio and centroid frequency shift methods. The sensitivity of attenuation analyses to different depth intervals, borehole irregularities, and different frequency ranges is also examined, to validate the stability of attenuation estimation. The final attenuation results indicate that high attenuation over the seismic frequency range (30–110 Hz) is associated with the presence of probable gas zones, while significant compressional attenuation was not observed in MH-bearing sediments at seismic frequencies. Zones of high compressional attenuation in the sonic frequency range (10–20 kHz) are affected by the presence of MH. Thus, this study demonstrated the frequency-dependence of attenuation in methane hydrates-bearing sediments.

Acknowledgments

References

Biot, M. A., 1956, Theory of propagation of elastic waves in a fluid saturated porous solid: *The Journal of the Acoustical Society of America* **28**, 168–191. doi:10.1121/1.1908239

Chand, S., and Minshull, T. A., 2004, The effect of hydrate content on seismic attenuation: A case study for Mallik 2L–38 well data, Mackenzie delta, Canada: *Geophysical Research Letters* **31**, L14609. doi:10.1029/2004GL020292

Dvorkin, J., and Uden, R., 2004, Seismic wave attenuation in a methane hydrate reservoir: *The Leading Edge* **23**, 730–734. doi:10.1190/1.1786892

Ecker, C., Dvorkin, J., and Nur, M. A., 2000, Estimating the amount of gas hydrate and free gas from marine seismic data: *Geophysics* **65**, 565–573. doi:10.1190/1.1444752

Gei, D., and Carcione, J. M., 2003, Acoustic properties of sediments saturated with gas hydrate, free gas and water: *Geophysical Prospecting* **51**, 141–157. doi:10.1046/j.1365-2478.2003.00359.x

Gist, G. A., 1994, Seismic attenuation from 3-D heterogeneities: A possible resolution of the VSP attenuation paradox: *64th Annual International Meeting, Society of Exploration Geophysicists*, 1042–1045.

Goupillaud, P. L., 1961, An approach to inverse filtering of near surface effects from seismic records: *Geophysics* **26**, 754–760. doi:10.1190/1.1438951

Guerin, G., and Goldberg, D., 2002, Sonic waveform attenuation in gas hydrate-bearing sediments from the Mallik 2L–38 research well, Mackenzie Delta, Canada: *Journal of Geophysical Research* **107**(No. B5), 2088. doi:10.1029/2001JB000556

Helgerud, M., Dvorkin, J., Nur, A., Sakai, A., and Collett, T., 1999, Elastic-wave velocity in marine sediments with gas hydrates: Effective medium modelling: *Geophysical Research Letters* **26**, 2021–2024. doi:10.1029/1999GL900421

Inamori, T., and Hato, M., 2004, Detection of methane hydrate-bearing zones from seismic data: *Resource Geology* **54**, 99–104.

Jannsen, D., Voss, J., and Theilen, F., 1985, Comparison of methods to determine Q in shallow marine sediments from vertical reflection seismograms: *Geophysical Prospecting* **33**, 479–497. doi:10.1111/j.1365-2478.1985.tb00762.x

Johnston, D. H., Toksöz, M. N., and Timur, A., 1979, Attenuation of seismic waves in dry and saturated rocks, II: Mechanisms: *Geophysics* **44**, 691–711. doi:10.1190/1.1440970

Kamei, R., Hato, M., and Matsuoka, T., 2004, Random heterogeneous model with bi-modal velocity distribution: *Exploration Geophysics* **36**, 41–49.

Korenaga, J., Holbrook, W. S., Singh, S. C., and Minshull, T. A., 1997, Natural gas hydrates on the Southeast U. S. margin: Constraints from full-waveform and travel time inversion of wide-angle seismic data: *Journal of Geophysical Research* **102**, 15345–15365. doi:10.1029/97JB00725

Lee, M. W., Hutchinson, D. R., Collett, T. S., and Dillon, W. P., 1996, Seismic velocities for hydrate-bearing sediments using weighted equation: *Journal of Geophysical Research* **101**, 20347–20358. doi:10.1029/96JB01886

Matsushima, J., 2004, Attenuation measurements from sonic waveform logs in methane hydrate-bearing sediments at the Nankai Trough exploratory well off Tokai, central Japan: *Geophysical Research Letters* **32**, L03306. [Correction, *Geophysical Research Letters*, **33**, L02305, 2006.]

Matsushima, J., 2006, Seismic wave attenuation in methane hydrate-bearing sediments: Vertical seismic profiling data from the Nankai Trough exploratory well, offshore Tokai, central Japan: *Journal of Geophysical Research* **111**, B10101. doi:10.1029/2005JB004031

Pratt, R., Bauer, K., and Weber, M., 2003, Crosshole waveform tomography velocity and attenuation images of arctic gas hydrates: *73rd Annual International Meeting, Society of Exploration Geophysicists, Extended Abstracts*, 2255–2258.

Pujol, J., and Smithson, S., 1991, Seismic wave attenuation in volcanic rocks from VSP experiments: *Geophysics* **56**, 1441–1455. doi:10.1190/1.1443164

Quan, Y., and Harris, M. J., 1997, Seismic attenuation tomography using the frequency shift method: *Geophysics* **62**, 895–905. doi:10.1190/1.1444197

Sloan, E. D., 1990, *Clathrate Hydrates of Natural Gases*, Marcel Dekker.

Stainsby, D. S., and Worthington, H. W., 1985, Q estimation from vertical seismic profile data and anomalous variations in the central North Sea: *Geophysics* **50**, 615–626. doi:10.1190/1.1441937

Staykova, D. K., Kuhs, W. F., Salamatin, A. N., and Hansen, T., 2003, Formation of porous gas hydrates from ice powders: diffraction experiments and multistage model: *Journal of Physical Chemistry B* **107**, 10299–10311. doi:10.1021/jp027787v

Tsuji, Y., Ishida, H., Nakamizu, M., Matsumoto, R., and Shimizu, S., 2004, Overview of the MITI Nankai Trough Wells: A milestone in the evaluation of methane hydrate resources: *Resource Geology* **54**, 3–10.

Walsh, J. B., 1966, Seismic attenuation in rock due to friction: *Journal of Geophysical Research* **71**, 2591–2599.

Walsh, J. B., 1969, New analysis of attenuation in partially melted rock: *Journal of Geophysical Research* **74**, 4333–4337.

Wood, W. T., Stoffa, P. L., and Shipley, T. H., 1994, Quantitative detection of methane hydrate through high-resolution seismic velocity analysis: *Journal of Geophysical Research* **99**, 9681–9695. doi:10.1029/94JB00238

メタンハイドレート賦存層において VSP 記録から得られた地震波減衰

松島 潤

要 旨： メタンハイドレート賦存層 (MH 層) は地震波を減衰させることが最近の観測より示唆されている。メタンハイドレートの賦存が確認されている東海沖の基礎試錐「南海トラフ」にて取得された VSP 記録を用いて周波数帯域 30-110Hz における地震波減衰を評価した。減衰解析には Spectral Ratio 法と Centroid Frequency Shift 法を比較適用し，さらに散乱減衰効果を除去するために音波検層ならびに密度検層から得られる音響インピーダンス構造を用いて多重反射を考慮した一次元数値モデリングデータを作成し，フィールドデータから得られた減衰値から数値データから得られた減衰値を差し引いた。当該周波数帯域では，MH 層における顕著な減衰は確認できず，むしろ低飽和ガス層において最大減衰値が確認された。解析深度区間，周波数帯域，坑径変化が減衰解析結果に及ぼす影響を評価して，解析結果の妥当性を確認した。当該坑井において実施された音波検層波形を用いて実施された減衰解析では，メタンハイドレート賦存層における減衰値は顕著であったことを考えるとメタンハイドレート賦存層における減衰特性は周波数依存性を有していることが推定される。ただし，MH 層の層厚が薄いことにより，周波数帯域 30-110Hz では有意な減衰値が得られなかったことも理由として考えられる。

キーワード： メタンハイドレート，地震波減衰，VSP，フリーガス，南海トラフ

메탄 하이드레이트 부존 퇴적층으로부터 획득한 수직탄성파 (VSP) 자료에서의 탄성파 진폭 감쇠

Jun Matsushima

요 약： 최근의 탄성파 탐사들은 퇴적층에 메탄 하이드레이트가 존재할 경우 탄성파 진폭 감쇠에 큰 영향을 미치는 것을 보여주고 있다. 이 논문에서는 일본 중부 토카이 (Tokai) 해역의 난카이 트러프 (Nankai Trough) 탐사정에서 얻은 수직탄성파자료를 이용하여 30 ~ 110 Hz 주파수 대역에서 메탄 하이드레이트 부존층에서의 P 파 감쇠를 측정하였다. 두 개의 다른 측정방법들 (스펙트럼비 (spectral ratio) 방법과 중심 주파수 이동방법 (centroid frequency shift method))을 이용하여 감쇠 측정의 유효성을 조사하였다. 또한 감쇠 측정의 안정성을 증명하기 위해 측정 심도구간, 시추공의 불규칙 변화, 주파수 구간에 따른 감쇠 분석의 민감도를 조사하였다. 탄성파 주파수 대역에서는 메탄 하이드레이트 부존층에서 P 파의 큰 진폭 감쇠는 발견되지 않았다. 육안으로 보기에는 탄성파 주파수 대역에서의 최대 감쇠는 저포화도의 가스층에 발생한다. 그와는 반대로 같은 시추공에서 얻어진 음파검층의 주파수 대역 (10 ~ 20 kHz)에서는 가장 높은 P 파의 진폭 감쇠가 메탄 하이드레이트 부존층과 관련이 있었다. 그러므로 이 연구는 메탄 하이드레이트 부존 퇴적층의 진폭 감쇠가 주파수에 의존함을 보여주고 있다. 메탄 하이드레이트 부존층은 탄성파 주파수 대역보다는 음파검층 주파수 대역에서 진폭 감쇠를 유발함을 알 수 있다. 30 ~ 110 Hz 의 탄성파 주파수 대역이 메탄 하이드레이트 부존에 영향을 받지 않는 이유 중의 하나로서 메탄 하이드레이트 지역의 얇은층 들로 이루어진 층서구조의 영향을 제시하였다.

주요어： 메탄 하이드레이트, 감쇠, 수직탄성파탐사 (VSP), 자유 가스, 난카이 트러프 (Nankai Trough)

東京大学大学院工学系研究科地球システム工学専攻   도쿄대학 대학원 공학계 연구과 지구 시스템공학 전공
〒113-8656 東京都文京区本郷 7-3-1